

Emerging attractors and the transition from dissipative to conservative dynamics

Christian S. Rodrigues*, Alessandro P. S. de Moura, and Celso Grebogi

*Department of Physics, King's College, University of Aberdeen - Aberdeen AB24 3UE, UK. and
Institute for Complex Systems and Mathematical Biology,*

King's College, University of Aberdeen - Aberdeen AB24 3UE, UK.

(Dated: November 7, 2018)

The topological structure of basin boundaries plays a fundamental role in the sensitivity to the final state in chaotic dynamical systems. Herewith we present a study on the dynamics of dissipative systems close to the Hamiltonian limit, emphasising the increasing number of periodic attractors, and on the structural changes in their basin boundaries as the dissipation approaches zero. We show numerically that a power law with nontrivial exponent describes the growth of the total number of periodic attractors as the damping is decreased. We also establish that for small scales the dynamics is governed by *effective* dynamical invariants, whose measure depends not only on the region of the phase space, but also on the scale under consideration. Therefore, our results show that the concept of effective invariants is also relevant for dissipative systems.

PACS numbers: 05.45.Ac 61.43.Hv

I. INTRODUCTION

Many dynamical processes have been shown to possess coexisting metastable states, and their dynamics can be highly sensitive to the initial conditions. Some examples include neural behaviour [1, 2], rain events [3], earthquakes' dynamics [4, 5], effective fractal dimension of energy levels [6], among others. Their correct interpretation requires an understanding of dynamical systems with very low dissipation, lying in between the strongly dissipative limit and the conservative one. In spite of the importance of this problem, there are few systematic studies of the low-dissipation limit and the transition from dissipative to conservative dynamics. This is the problem we address in this paper.

In Hamiltonian systems, chaotic regions typically coexist with regions of regular motion around the marginally stable periodic orbits, also known as Kolmogorov-Arnold-Moser (KAM) invariant tori. Chaotic trajectories have intermittent behaviour and spend long times sporadically near the border of regular islands. This stickiness to the KAM tori makes their dynamics fundamentally different from that of hyperbolic chaotic systems, since even small islands can exert great influence on the global dynamics [7, 8, 9]. On the other hand, strongly dissipative systems are characterised as having only one or few attractors to which all the initial conditions eventually converge. These two regimes could not be more different from each other; however, if the dissipation decreases to zero, the phase space structure of the dissipative systems must evolve in such a way as to approach the complex hierarchical organisation found in Hamiltonian systems. How this transformation occurs is far from obvious.

Despite the existence of extensive investigations on strongly dissipative and on Hamiltonian systems, very

little is known about properties of systems close to the border between dissipative and conservative dynamics, where many coexisting periodic attractors are present [10]. In this paper we investigate the growth of the number of periodic attractors and how the topology of the phase space evolves when the dissipation is reduced. We obtain numerically a power law describing the growth of the number of periodic attractors as the damping approaches zero. When the system is close to the Hamiltonian limit, we find that high-period periodic attractors become increasingly important in the system's dynamics, in contrast to the case with high dissipation. These *emerging attractors* proliferate ever more rapidly as the dissipation decreases. Moreover, we argue that although this number can be extremely high for small dissipation, we expect it to be finite (for non-zero dissipation), as conjectured recently [11, 12]. The power law of the number of attractors with dissipation, found in this work, corroborates this conjecture. Another important finding in this paper is that for low levels of damping the dynamics is characterised by *effective invariants*, a concept previously used in the context of non-hyperbolic dynamics of Hamiltonian systems [7]. We study specifically the *effective fractal dimension*, which we show to depend on the scale and also on the region of the phase space. Therefore we show that effective dynamics is relevant also for dissipative systems, and not only for Hamiltonian ones.

This paper is organised as follows. We start, with Sec. II, where we introduce the dynamical systems used in our analysis and revisit the problem of the number of coexistent periodic attractors. It is followed, Sec. III, by a discussion regarding the topology of the phase space in the low-dissipation limit. In Sec. IV we introduce effective invariants and define the effective fractal dimension for weakly dissipative systems. Finally, Sec. V brings our conclusions. In the appendix, we bring up some formal definitions. In particular, we recall a definition of *periodic attractors*, and discuss its implications for both experi-

*Electronic Address: c.rodrigues@abdn.ac.uk

mental and numerical realistic investigations, where one typically is only able to make use of limited precision. We also recall a definition of *basin of attraction*, which is coherent with the definition of periodic attractors used here.

II. NUMBER OF PERIODIC ATTRACTORS

A. Single Rotor Map

A paradigmatic system that allows the investigation of the transition from the dissipative to the conservative limit is the *single rotor map*, obtained from the mechanical pendulum kicked periodically at times nT , $n \in \mathbb{N}^+$, with force f_0 [13]:

$$\begin{aligned} x_{n+1} &= x_n + y_n \pmod{2\pi} \\ y_{n+1} &= (1 - \nu)y_n + f_0 \sin(x_n + y_n), \end{aligned} \quad (1)$$

where $x \in [0, 2\pi]$ corresponds to the phase, $y \in \mathbb{R}$ to the angular velocity, and $\nu \in [0, 1]$ is the damping parameter. For $\nu = 0$, the well known area preserving standard map analysed by Chirikov [14] is recovered. For $\nu = 1$, we obtain the circle map with zero rotation number.

Previous work has considered the question of the number of attractors for this system [10]. They have derived an analytical expression for the number of period-1 primary attractors, that have not undergone period doubling bifurcation:

$$N_{p1} = 2I\left(\frac{f_0}{2\pi\nu}\right) + 1, \quad (2)$$

where $I(\cdot)$ denotes the integer part of the expression in brackets. As pointed out in Ref. [10], numerical detection of attractors with high period is a difficult task. The reason is the extremely small size of their basins of attraction, what requires computation using very fine grids. Adding to this, they have short lifetime in the space of parameters. Therefore it is necessary to follow a great number of initial conditions in order to be able to detect them.

Here we overcome this problem. Instead of choosing an *a priori* fixed number of initial conditions in a preset grid, as previously done in Ref. [10] and elsewhere, we fix the non linearity $f_0 = 4.0$ for a given damping ν and then iterate an ensemble of randomly chosen initial conditions with uniform distribution on a bounded region of the phase space. Therefore, the chance for an attractor to be found does not depend on our particular choice of the grid. For the dissipative case the dynamics takes place in the cylinder $\Gamma = [0, 2\pi] \times \mathbb{R}$ and the area where the initial conditions are chosen depends on the damping. Since $\nu > 0$, from the second equation in the map (1), one gets $|y_{k+1}| \leq (1 - \nu)|y_k| + f_0$, so if $|y_k| > f_0/\nu \Rightarrow |y_{k+1}| < |y_k|$. Hence the attractors are found in $\Lambda \subset \Gamma$, with $\Lambda = [0, 2\pi] \times [-y_{max}, y_{max}]$, where $y_{max} = f_0/\nu$.

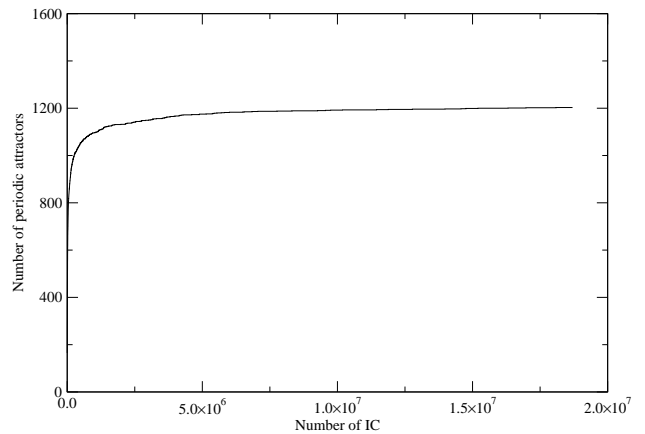


FIG. 1: Total number of periodic attractors detected for a specific value of the dissipation ν , as a function of the number of initial conditions randomly chosen in Λ and evolved according to the map. The parameters for the map (1) were $f_0 = 4.0$, and $\nu = 0.0035$.

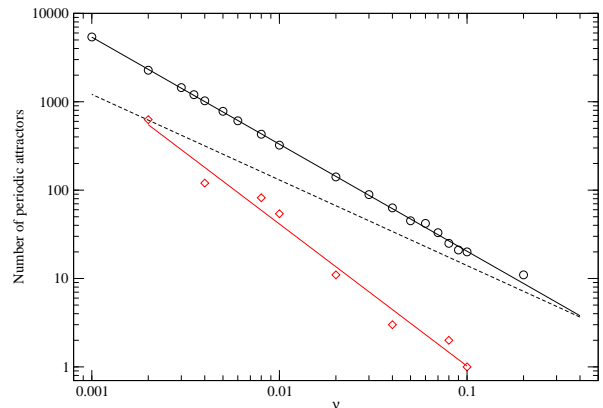


FIG. 2: (Colour online) Total number of periodic attractors which were detected numerically for the single rotor map (black circles), and for the Hénon map (red diamonds) for different values of ν . The parameters were $f_0 = 4.0$, for the single rotor map, and $A = 1.075$ for the Hénon map. It is also shown the power laws fits, the black and the red solid lines for the single rotor map and for the Hénon map, respectively; compare to the number of period 1 attractors expected from Eq. (2) (black dashed line) for the single rotor map. The divergence from this curve (dashed black line) to the other (black solid line) is clear, showing the important contribution of high period periodic attractors in the regime of small damping for the single rotor map.

In order to detect the attractors, even with very small basins of attraction, we keep iterating new, randomly chosen initial conditions $(x_0, y_0) \in \Lambda$ until their trajectories converge to some periodic attractor. We use up to 2×10^5 iterations; independently of the damping, this provides a convergence of more than 99.5% of the initial conditions. We have ignored the remaining trajectories (which may include chaotic orbits), regarding them as

not being statistically representative. It is known that for this and similar systems, almost all attractors consist of periodic orbits. We keep iterating new initial conditions until we fail to find new attractors. This was determined by the criterion that whenever the total number of detected attractors did not change for the last 10^6 initial conditions, we assume that all the detectable attractors have been found. This is illustrated in Fig. 1 for $\nu = 0.0035$. We repeat this procedure for different values of ν , in order to find how the total number of periodic attractors changes with damping. Notice that the area of the phase space where the trajectories are trapped grows as we decrease ν ; for $\nu = 0.001$ for example, we need 22×10^6 initial conditions to find most attractors in the system.

The question regarding the finiteness of the number of attractors and their density in phase space has been considered before and it is widely regarded as one of the most important open problems still to be answered in Dynamical Systems Theory [11]. Among many conjectures, it has been initially proposed that the number of attractors was infinite [15]. Afterwards it has been proved that this should only hold for a zero measure set of parameter values, though dense in some interval [16]. Recently it has also been conjectured by Palis that the total number of attractors should be finite [12].

To investigate this issue using our system (1) as a testing ground, we calculate the number of attractors as described above, and see how this depends on the dissipation ν as it is decreased and approaches the conservative limit, i.e. $\nu \rightarrow \varepsilon > 0$. Figure 2 shows a *log-log* plot of our data, yielding a power law describing the dependence of the total number of periodic attractors on ν .

Numerical fitting gives us the following law:

$$N_{TP_R} \approx 1.26 \cdot \nu^{-1.21}, \quad (3)$$

where N_{TP_R} is the total number of detected periodic attractors for the map (1).

Now we want to compare our power law for the growth of the total number of periodic attractors with the formula (2) [10] for the number of period 1 attractors. We observe in Fig. 2 that when the damping is decreased the contribution of higher period periodic attractors becomes important for the total number of detected attractors. The main reason is that the *lifetime* of a stable, periodic orbit in parameter space increases as damping is reduced. By *lifetime* of an orbit we mean the range in parameter space for which the orbit exists, without undergoing any bifurcation. Since the higher the period of an attractor, the smaller its lifetime interval in parameter space [10], the extension of lifetime for small damping promotes the overlap of different periodic orbits in the space of parameters, which was not possible before. Equation (2) is only valid within the parameter intervals where none of the period 1 attractors has undergone period doubling [10]. Since some of the period 1 attractors may have gone through such process for the parameters in Fig. 2, the difference between the expected

number of period 1 attractors and the total number of attractors can be even larger than that inferred from the above argument.

B. The Hénon Map

We further investigated the growth of the number of periodic attractors for a map of a different class than the previous one. We chose the Hénon map in the form [17]:

$$\begin{aligned} x_{n+1} &= A - x_n^2 - (1 - \nu)y_n \\ y_{n+1} &= x_n, \end{aligned} \quad (4)$$

where A represents the bifurcation or non linearity control parameter. The parameter $\nu \in [0, 1]$ represents the damping parameter. When $\nu = 1$, the two equations in Eq. 4 are no longer coupled, and we obtain the quadratic map. For the other limit, $\nu = 0$, we have a conservative map, hence the determinant of its Jacobian matrix is equal to 1. Contrary to the case for the map (1), the dynamics for the Hénon map (4) is not *a priori* contained within a region of the phase space. For a range of parameters, the initial conditions can either be trapped by some of the coexistent periodic attractors, or be scattered. In fact, most of the initial conditions diverge to infinity.

We repeated the procedure applied to the previous map in order to obtain the number of periodic attractors for the Hénon map. We fixed $A = 1.075$ for the map (4), and we iterated a set of initial conditions in $[-5, 5] \times [-5, 5]$ verifying whether they converged to some periodic attractor or diverged. Because the number of initial conditions converging to periodic attractors is much smaller than that diverging, in order to obtain about 20×10^6 initial conditions converging to periodic motion, as many as 20×10^7 initial conditions were necessary depending on the damping.

Figure 2 shows a *log-log* plot of our data, yielding a power law describing the dependence of the total number of periodic attractors on ν . For the Hénon map, the numerical fitting produces:

$$N_{TP_H} \approx 0.025 \cdot \nu^{-1.61}, \quad (5)$$

where N_{TP_H} is the total number of detected periodic attractors for the map (4).

As previously observed [17], the Hénon map belongs to a class of dynamical systems whose the conservative element has few primary island, which are surrounded by secondary ones. Therefore, although it also observed the coexistence of periodic attractors for a range of parameter, it is expected this number to be smaller than that for the single rotor's family.

C. On the General Behaviour

Even though we cannot claim the above result to be a mathematical proof, our results seem to uphold Palis'

conjectures [11, 12], i.e., for any arbitrarily small $\varepsilon > 0$, the limit of Eqs. (3), [(5)], as $\lim_{\nu \rightarrow \varepsilon^+} N_{TP_{R,[H]}}$ predicts a finite number of attractors for the system, though this number can be very high for small ε (N_{TP_R} , and N_{TP_H} for the single rotor map, and for the Hénon map, respectively).

Although some attractors may have their basins of attraction so tiny that even by iterating a huge number of initial conditions is not enough to numerically detect them. Figure 1 shows that the number of attractors which was detected is asymptotic to a constant (we obtain a similar figure for the Hénon map). Therefore, our results indicate that the number of attractors increases as a power law as the dissipation decreases, being finite for any given $\nu > 0$, though arbitrarily large for ν approaching zero. Even though the specific value of the exponent in Eq. (3) and Eq. (5) may be only valid for the map (1), and the map (4), respectively, the growth of the number of periodic attractors is a very generic property of weakly dissipative systems [17] which should not depend on the details of the system, since in the low-dissipative limit the system's phase-space approaches that of Hamiltonian systems, which have universal properties. We therefore expect that the same behaviour to hold for other systems.

If we follow the distributions of filaments of the largest basin of attraction in the phase space, we notice that their structure becomes more heterogeneous for different regions when the damping is decreased. This is illustrated in Fig. 3, where each colour (colour online) represents a set of initial conditions which converge to one of the attractors, i.e., different colours represent different basins of attraction. In Fig. 3 (a), for which $\nu = 0.32$, we notice that the largest basin of attraction (in black) is spread out over the phase space in an intricate structure. Moreover, if we compare distinct regions of the phase space, there is a qualitative difference in the “density” of filaments of the largest basin of attraction. In particular, the farther the region is from the main attractor, the thinner the filaments become. In Fig. 3 (b), for $\nu = 0.3$, we detect five attractors and the topology of the phase space, i.e., the spatial distribution of invariant sets, seems to become more complex. Going even further, for $\nu = 0.2415$ in Fig. 3 (c), we have seven attractors in the same region and the difference of density of those filaments is clearer. Figure 3 (d) is the blow up of the region $x \in [4, 5], y \in [-15, -10]$ for $\nu = 0.2415$. The rescaling of the phase space shows the structure of the basins which seems to form a self similar pattern, as illustrated in Fig. 4.

As we decrease the damping even further, this process seems to carry on and the heterogeneity of the phase space keeps increasing. Furthermore, the difference in density of filaments of distinct regions of the phase space is seen by looking, for instance, at the largest

The natural question which arises is the following: what happens to the topology of the phase space as new attractors continually appear with decreasing damping?

III. TOPOLOGY OF THE PHASE SPACE

We start this section by presenting a qualitative picture of the transformations occurring in phase space structure when the damping is decreased. For simplicity, we restrict ourselves to the map (1). Although one cannot draw definitive conclusions from this qualitative analysis, it motivates us to some further quantitative investigation, which will be tackled at the end of this section and in the next one. In order to get some clue about which topological changes occur when the damping is decreased, we begin by looking at the phase space for the system with constant forcing and high damping. In this case the system has only few periodic attractors. We decrease then ν , find the periodic attractors for the new parameter and plot their basins of attraction. Since we are now only interested in the general picture, the number of initial conditions is fixed at 2×10^6 .

basin of attraction for $\nu = 0.02$, and $f_0 = 4.0$. For these parameters we expect from Eq. (3) to find about 140 periodic attractors. The largest basin of attraction is responsible for about 36% of the initial conditions $(x_0, y_0) \in [0, 2\pi] \times [-\pi, \pi]$ [10]. This is illustrated in Fig. 5, which has been done by the iteration of an ensemble of 10^6 initial conditions.

The structures we just presented are nothing but manifestations of some of the underlying invariant sets. That is, the dynamics has multiple periodic attractors, and the closure of the set of initial conditions that approaches a give attractor is its basin of attraction. The boundary which separates different basins of attraction is the basin boundary. This basin boundary is the stable manifold of an invariant set. If we define the boundary B in some region of the phase space embedded in the boundary as $S \cap B$, where S denotes some open set in phase space which contains part of the boundary B , we expect for a given ν the fractal dimension of the basin boundary, $dim(S \cap B)$, to be constant at different regions of the phase space, $\mathbf{R} \subset \mathbf{\Gamma}$, as it has been conjectured in Ref. [18]. Nevertheless, for physically relevant scales, the heterogeneity in the distribution of the basins over the phase space, and hence the spatially heterogeneous distribution of invariant manifolds, suggests that course-grained measurements of quantities such as the fractal dimension should lead to different results depending on the region of the phase space and on the scale under consideration. The reason is that realistic measurements never take the limit of infinitely small scales,

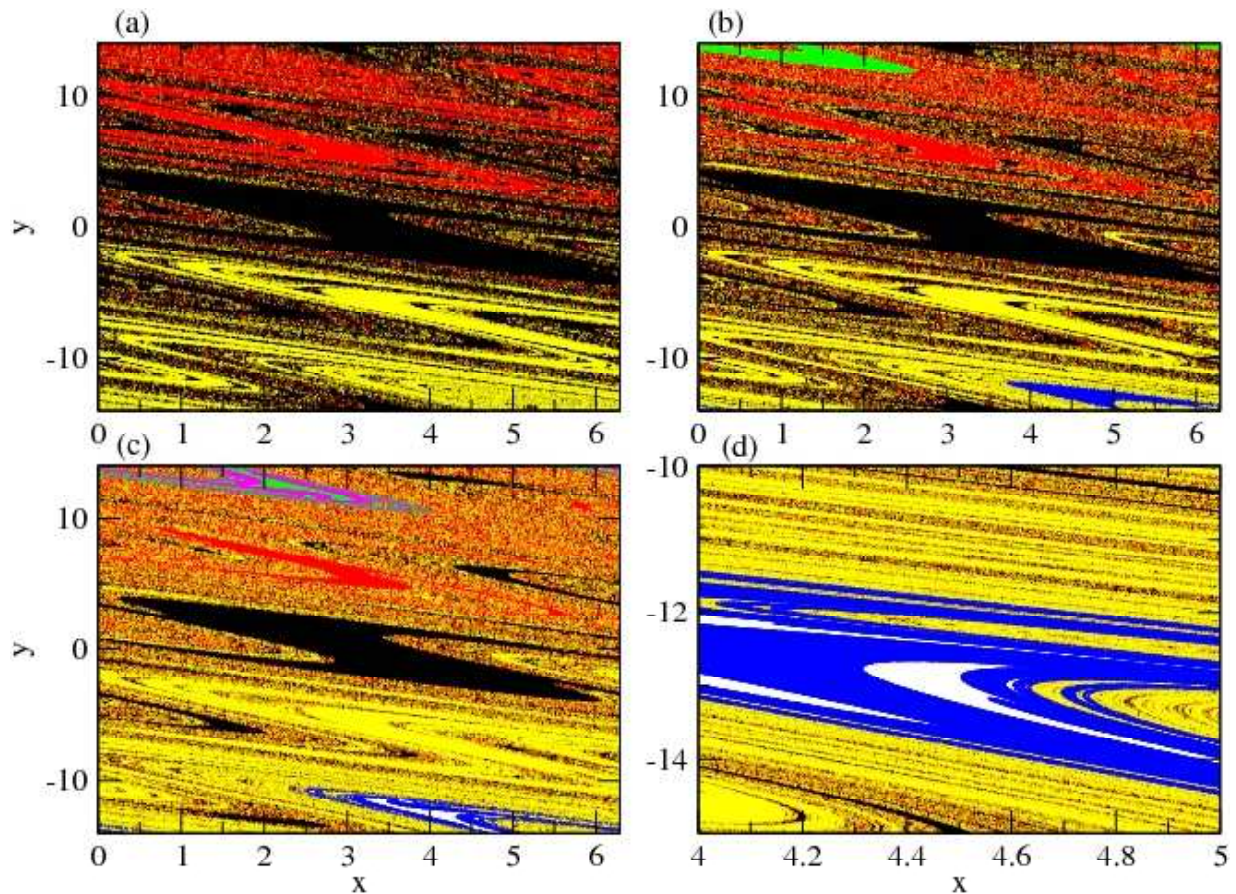


FIG. 3: (Colour online) Basins of attraction for $f_0 = 4.0$ at different values of ν . Each colour represents a set of initial conditions which converge to one of the attractors. In (a) $\nu = 0.32$, in (b) $\nu = 0.3$, in (c) $\nu = 0.2415$, and (d) is the blow up of a region $x \in [4, 5]$, $y \in [-15, -10]$ for $\nu = 0.2415$. We used 2×10^6 initial conditions for each one of the figures.

but must have a finite lower scale. Previous works in the context of Hamiltonian systems show that when the phase space has a heterogeneous structure such as in this

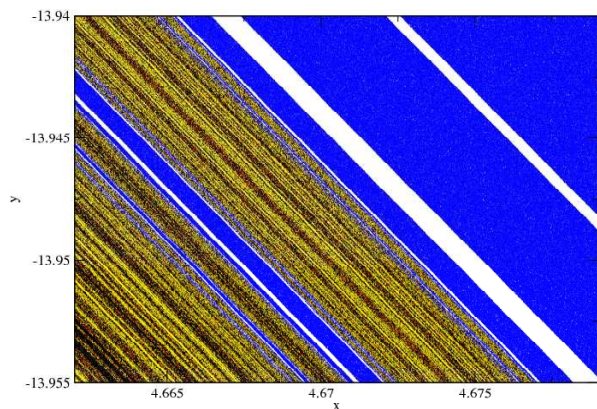


FIG. 4: (Colour online) Blow up of the region $x \in [4.662, 4.679]$, $y \in [-13.955, -13.94]$ for $\nu = 0.2415$ in Fig. 3 (d), showing the fractal Cantor structure.

case, one needs to go to exceedingly small scales to approach the mathematical value of the fractal dimension, which is unique and independent of the portion of the phase space used to calculate it. For physically realistic scales, an approximation to the fractal dimension (and similar quantities) is more appropriate to describe the system's dynamics; this approximation, called the *effective fractal dimension*, depends on the position as well as on the scale under consideration. This effective fractal dimension will be presented in more detail in the next section.

A finite-scale approximation of the fractal dimension of the basin boundary can be estimated using the uncertainty method [19]. It consists in iterating an ensemble of initial conditions (x_0, y_0) and checking to which attractor they converge. Then we add a small perturbation ε to every initial condition, say $(x_0, y_0 + \varepsilon)$, and check whether they change from one basin to another. We count the fraction of initial conditions that have changed their asymptotic state after being perturbed in this manner. This fraction, $f(\varepsilon)$ of ε -uncertain points is the fraction of initial conditions that change basins under an ε -size perturbation, and it scales as $f(\varepsilon) \sim \varepsilon^\alpha$, where α

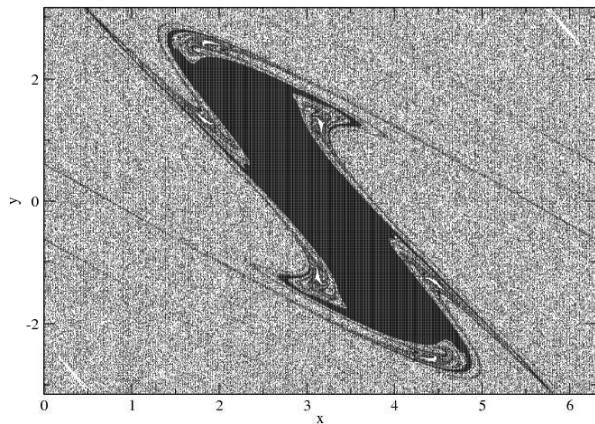


FIG. 5: The largest basin of attraction for $\nu = 0.02$ and $f_0 = 4.0$. The black points represent initial conditions which converge to the attractor formed from the main island. The initial conditions were chosen such that, $(x_0, y_0) \in [0, 2\pi] \times [-\pi, \pi]$. We used the same parameters as those used in Ref [10].

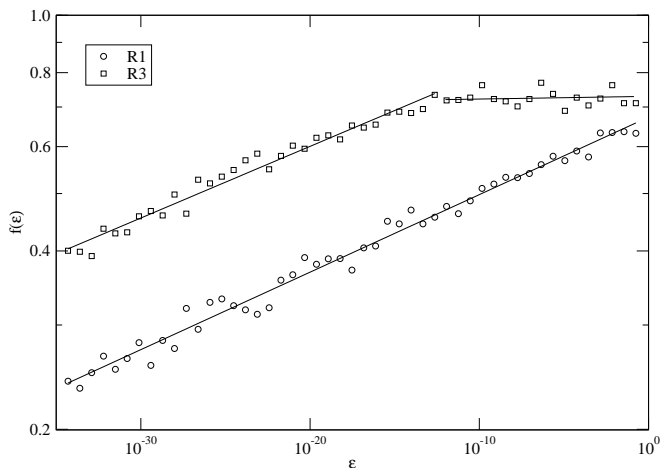


FIG. 6: Fraction of uncertain initial conditions $f(\varepsilon)$ as a function of the perturbation size ε for two different regions of the phase space. The regions, $\mathbf{R}_i \subset \mathbf{\Gamma}$, were defined as $\mathbf{R}_1 \equiv (x, y) \in [0, 1.5] \times [-1.0, -2.5]$, and $\mathbf{R}_3 \equiv (x, y) \in [1.0, 2.5] \times [198.5, 200.0]$. The utilised parameters were $f_0 = 4.0$, and $\nu = 0.08$.

is related to the box counting dimension d of the basin boundary by $\alpha = D - d$, where D is the dimension of the phase space (For the map (1) we have $D = 2$).

In Fig. 6 we show the fraction of “uncertain” initial conditions as function of the size of perturbation ε [20]. The slope of the curves are related to the fractal dimension of the basin boundary.

The exponents $\alpha = \Delta \ln f(\varepsilon) / \Delta \ln \varepsilon$ can be computed over some decades. However, we notice in Fig. 6 that the slope assumes different values for distinct regions of the phase space. Such regions, $\mathbf{R}_i \subset \mathbf{\Gamma}$, are defined as $\mathbf{R}_1 \equiv (x, y) \in [0, 1.5] \times [-1.0, -2.5]$, and $\mathbf{R}_3 \equiv (x, y) \in$

$[1.0, 2.5] \times [198.5, 200.0]$, and they were chosen with the same Lebesgue measure. We chose three different regions of the phase space, located at different distances from the main attractor. We remark that, although such regions may be out of $\mathbf{\Lambda} \subset \mathbf{\Gamma}$ defined in section II, it does not follow that they do not contain boundaries. This is because regions $\mathbf{\Lambda} \subset \mathbf{\Gamma}$, defined for each value of ν , are portions of the phase space where the attractors are to be found; their basins, on the other hand, are expected to be extended throughout the phase space. Since the density of periodic attractors in phase space decreases when we look at regions farther away from the main attractor, we expect the stable manifold to be denser around the central part of the phase space. Furthermore, given that we expect the dissipative regime to approach the complex structures of the Hamiltonian dynamics at the zero dissipation limit, it is sensible to expect a distribution of manifolds which are similar for conservative and for low dissipative dynamics. For Hamiltonian dynamics, the density of manifolds decreases as one looks at regions farther from the main island [7].

Looking at Fig. 6, it is clear that for $\varepsilon > 10^{-13}$, the estimated fractal dimension is larger for the region \mathbf{R}_3 , where we expect the stable manifold to be less dense. Only when we go down to $\varepsilon < 10^{-13}$ does the slope for the region \mathbf{R}_3 converges to the same value as the one of the region \mathbf{R}_1 : for small enough ε , the slope eventually converges to the true fractal dimension, which has a unique value [18]. We have computed $f(\varepsilon)$ for even smaller values of ν , and we have observed the same behaviour. However, for values as small as $\nu = 0.02$, even going down to $\varepsilon = 10^{-35}$ is not enough to obtain a convergence to a unique value of the estimated dimension in different regions. This shows that an effective dimension is indeed the relevant physical quantity to be considered also for weakly dissipative systems.

IV. EFFECTIVE FRACTAL DIMENSION

From the theoretical results regarding the fractal dimension of the basin boundary [18], we expect to have the same fractal dimension for different regions of the phase space. However, the above discussion and results suggest that, for realistic scales, the behaviour for weakly dissipative systems can be quite different from the asymptotic one. Therefore it is sensible to describe the system in terms of *effective* invariants, a concept which has been used mostly in the context of non-hyperbolic Hamiltonian dynamical systems. [7]. As an example of effective invariants we use the definition of effective fractal dimension for a D -dimensional system, which depends on the region $\mathbf{R} \subset \mathbf{\Gamma}$, and on the scale under consideration [22]. It is defined as

$$D_{eff}(R, \varepsilon) = D - \left. \frac{d \ln f(\varepsilon')}{d \ln \varepsilon'} \right|_{\varepsilon'=\varepsilon}, \quad (6)$$

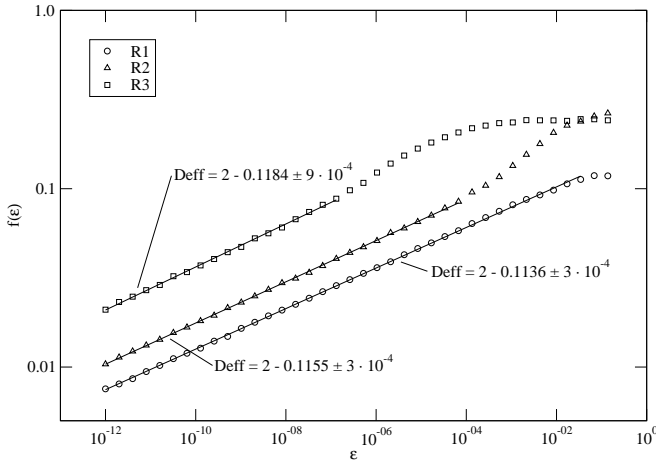


FIG. 7: Fraction of uncertain initial conditions $f(\varepsilon)$ scaling with the perturbation ε for three different regions of the phase space. The regions, $\mathbf{R}_i \subset \Gamma$, were defined as $\mathbf{R}_1 \equiv (x, y) \in [0, 1.5] \times [-1.0, -2.5]$, $\mathbf{R}_2 \equiv (x, y) \in [1.0, 2.5] \times [18.5, 20.0]$, and $\mathbf{R}_3 \equiv (x, y) \in [1.0, 2.5] \times [198.5, 200.0]$. The utilised parameters were $f_0 = 4.0$, and $\nu = 0.3$.

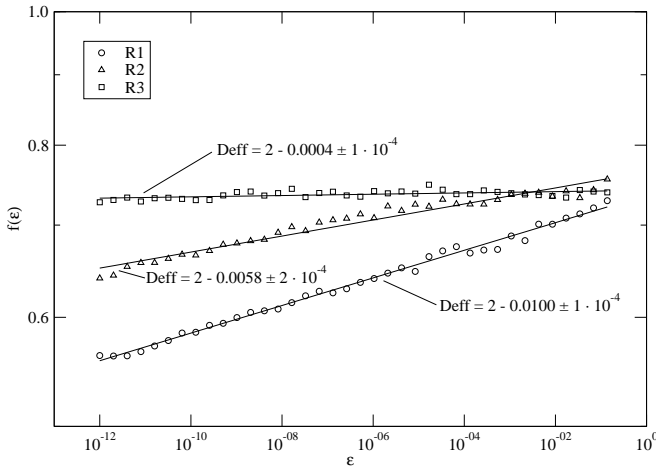


FIG. 8: Fraction of uncertain initial conditions $f(\varepsilon)$ scaling with the perturbation ε for three different regions of the phase space. The regions are the same as in Fig.7. The utilised parameters were $f_0 = 4.0$, and $\nu = 0.07$.

where $f(\varepsilon')$ is the total uncertain phase space volume estimated as $\varepsilon'^D N(\varepsilon')$, and $N(\varepsilon')$ is the number of hypercubes of size ε' necessary to cover $S \cap B$.

We have computed the effective fractal dimension of the basin boundary for finite scales, for different values of ν , and for distinct regions in the phase space. The regions, $\mathbf{R}_i \subset \Gamma$, were chosen to be $\mathbf{R}_1 \equiv (x, y) \in [0, 1.5] \times [-1.0, -2.5]$, $\mathbf{R}_2 \equiv (x, y) \in [1.0, 2.5] \times [18.5, 20.0]$, and $\mathbf{R}_3 \equiv (x, y) \in [1.0, 2.5] \times [198.5, 200.0]$.

We have extracted the effective fractal dimension from Fig. 7 for $\nu = 0.3$ and $f_0 = 4.0$, where the system has

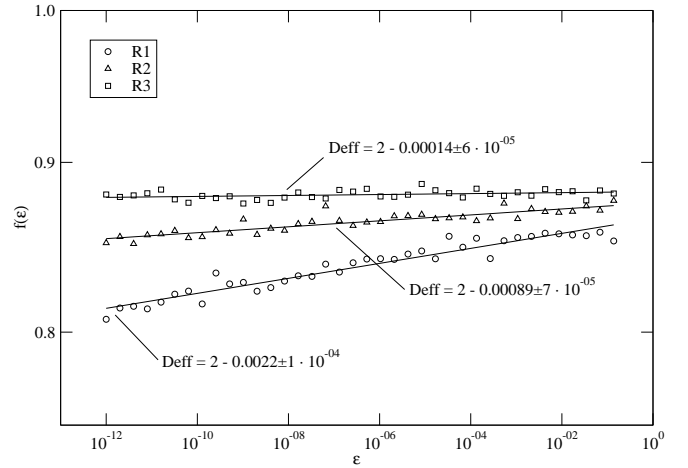


FIG. 9: Fraction of uncertain initial conditions $f(\varepsilon)$ scaling with the perturbation ε for three different regions of the phase space. The regions are the same as in Fig.7. The utilised parameters were $f_0 = 4.0$, and $\nu = 0.02$.

apparently 5 periodic attractors. We notice that for \mathbf{R}_3 , where the stable manifold is less dense, starting from $\varepsilon = 10^{-1}$, the value of the effective fractal dimension is larger, but after few decades it converges to nearly the same as for \mathbf{R}_1 , i.e., $D_{eff} = 1.89$, where the stable manifold is denser. The same phenomenon is observed for \mathbf{R}_2 , though the convergence is faster than for \mathbf{R}_3 . When we decrease ν , hence increasing the number of attractors, even for $\varepsilon = 10^{-12}$, which is almost in the limit of normal computation and far beyond realistic measurement capacity, we do observe different values of effective fractal dimension for different regions, as it is shown in Fig. 8 and Fig. 9, for $\nu = 0.07$ and $\nu = 0.02$, respectively. We also notice that for a given region the exponent α becomes smaller as the damping is decreased. This indicates that for such weakly dissipative systems, the fractal dimension is very close to the dimension of the phase space. This is, of course, in accordance with the fact that for Hamiltonian systems ($\nu = 0$), the fractal dimension assumes its maximum value, i.e., D .

V. CONCLUSION

We have shown that the dynamics of weakly dissipative dynamical systems can be quite different from either the strongly dissipative systems or the Hamiltonian ones. When the damping is decreased, the number of periodic attractors increases. We have shown that the growth of the total number of attractors is described by a power law. In general, the interval in the space of parameters in which an attractor exists is smaller for high period periodic attractors. For small damping, attractors with different periods coexist in phase space, and the contribution of high period periodic attractors to the dynamics becomes important. Although the total number of at-

tractors in the system is very high for low damping, our results strongly suggests that it remains finite for $\nu > 0$, supporting Palis' conjecture. The formation of new attractors as the damping decreases changes the topology of the phase space considerably. For low damping, the dynamics is better characterised by effective dynamical invariants, in a similar way to the case of non-hyperbolic Hamiltonian systems. These effective dynamical invariant sets depend on the scale and they differ from one region to the other in the phase space. In particular, the effective fractal dimension of the basin boundary is larger for regions where the stable manifold is less dense. For a given region, the smaller the damping, the closer the effective fractal dimension is to the dimension of the phase space. Although we have used a specific example to illustrate our ideas, our results are generic since we have deal only with general characteristics of dynamical systems close to Hamiltonian case [12].

Acknowledgments

The authors thank E. G. Altmann for the careful reading of the manuscript and useful suggestions. C. S. R. thanks I. J. Rodrigues for illuminating discussion, and takes the opportunity to pay his tribute to J. S. Rodrigues (*in memoriam*), who gave him the first scientific hints. This work was supported by the School of Natural Sciences, University of Aberdeen.

Appendix

On Periodic Attractors

Some of the most important characteristics of the dynamics are related to invariant subsets in the phase space, which attract their neighbouring points. These sets are called *attracting sets*, or *attractors*, depending on the context. There are various definitions for *attractor*, the main difference is related to which points in the neighbourhood must approach the set. We use the definition given for a *diffeomorphism* $f : \mathbb{R}^N \rightarrow \mathbb{R}^N$, that is f and its inverse are differentiable and the partial derivatives are continuous. The main source of our definition is Ref. [23].

The dynamics takes place in a phase space $\Gamma \subset \mathbb{R}^N$, where there is the notion of distance $dist(\mathbf{x}_1, \mathbf{x}_2)$ between points \mathbf{x}_1 and \mathbf{x}_2 , both belonging to Γ . For example, $dist(\mathbf{x}_1, \mathbf{x}_2)$ can be the *Euclidean distance* [24]. We say that a bounded and limited region of the phase space, i.e. $U_{\mathbf{A}} \subset \Gamma$ is called a *trapping region* for f if $f(U_{\mathbf{A}}) \subset int(U_{\mathbf{A}})$, where $int(U_{\mathbf{A}})$ stands for the interior of $U_{\mathbf{A}}$. Another important concept for the definition of *attractors* is the notion of ϵ -chain. An ϵ -chain of length n from \mathbf{x} to \mathbf{y} , for a map f is a sequence $\{\mathbf{x} = \mathbf{x}_0, \dots, \mathbf{x}_n = \mathbf{y}\}$, such that for all $1 \leq j \leq n$,

we have $dist(f(\mathbf{x}_{j-1}), \mathbf{x}_j) < \epsilon$. Now we are ready to

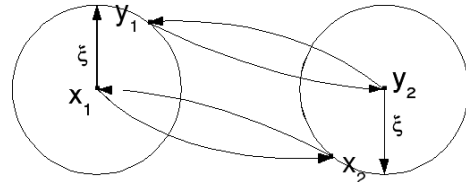


FIG. 10: Illustration of the dependence of the number of periodic attractors with the precision. The figure shows attractor x_i , and y_i , with $i = 1$, or 2 . Hence, the attractors are of period two. If on the detection of such attractors, $\epsilon > \xi$ is used, only one attractor of period 2 is detected. On the other hand, for $\epsilon < \xi$, we are able to distinguish them.

state a formal definition of *periodic attractors*. If forward iterating our map f in a trapping region, i.e. if we take the set $\mathbf{A} = \bigcap_{n \geq 0} f^n(U_{\mathbf{A}})$, and we eventually end up in an unique closed sequence of points such as these points are an ϵ -chain no matter how small $\epsilon > 0$ is, we have precisely what is defined as *attractor*. In some other words, a periodic attractor is the unique sequence of points $\{\mathbf{x}_1, \mathbf{x}_2, \dots, \mathbf{x}_p, \mathbf{x}_1\}$ remaining by iterating a trapping region, such that $dist(f(\mathbf{x}_{j-1}), \mathbf{x}_j) < \epsilon$, for all $\epsilon > 0$. In this case, we have *period* p . Notice that the attractivity of the attractor is ensured by requiring the existence of the trapping region. Furthermore, we remark that, finding multiple periodic attractors require the coexistence of different trapping regions.

Although the formal definition of attractor requires the existence of such sequence of points, the ϵ -chain, for all $\epsilon > 0$, and infinitely many iterations, both experimentally, and numerically, we are constrained by limited precision. Hence we are forced to use a mild condition on ϵ . Therefore, the number of periodic attractors obtained in realistic investigation intrinsically depends on the precision that we choose. We give a picturesque illustration of it in Fig 10. On determining of the number of periodic attractors in this paper, we have used $\epsilon = 10^{-10}$. Nevertheless, it does not minimise the importance of our findings, showing fundamental characteristics of the dynamics within realistic scale.

We also use a more general definition of *basin of attraction*. The *basin of attraction* of some trapping region U is the set of positive Lebesgue measure of initial conditions, whose orbits eventually enter U , as defined in Ref. [25]. Note that this slightly different definition avoids problems of coherence for not having an infinitely small ϵ . Because any periodic attractors is contained in some trapping region, hereafter we often mention the *basin of attraction* of some attractor, and it is understood the basin of a given trapping region containing the attractor under consideration.

-
- [1] N. Nagao, H. Nishimura, and N. Matsui, *Neural Processing Lett* **12**, 267 (2000).
- [2] S. J. Schiff and K. Jerger and D. H. Duong and et al., *Nature* **370**, 615 (1994).
- [3] O. Peters, and K. Christensen, *Phys. Rev. E* **66**, 036120 (2002).
- [4] P. Bak, K. Christensen, L. Danon, and T. Scanlon, *Phys. Rev. Lett* **88**, 178501-1 (2002).
- [5] M. Anghel, *Chaos Solit & Frac* **19**, 399 (2004).
- [6] W. F. Wang, and P. P. Ong, *Phys. Rev. A* **55**, 1522 (1997).
- [7] A. Motter, A. P. S. de Moura, C. Grebogi, and H. Kantz, *Phys. Rev. E* **65**, 026120 (2005).
- [8] J. D. Meiss, J. R. Cary, J. D. Crawford, C. Grebogi, A. K. Kaufman, and H. D. I. Abarbanel, *Physica D* **6**, 375 (1983).
- [9] E. G. Altmann, A. Motter, and H. Kantz, *Phys. Rev. E* **73**, 026207 (2006).
- [10] U. Feudel, C. Grebogi, B. R. Hunt, and J. A. Yorke, *Phys. Rev. E* **54**, 71 (1996).
- [11] J. Palis, *A global perspective for non-conservative dynamics*, Institute of Pure and Applied Mathematics (IMPA), preprint, 2005. See also references therein.
- [12] J. Palis, *Astérisque* **261**, 335 (2000).
- [13] G. M. Zaslavskii, *Phys. Lett. A* **69**, 145 (1978).
- [14] B. Chirikov, *Phys. Rep. A* **52**, 265 (1979).
- [15] S. E. Newhouse, *Topology* **13**, 9 (1974).
- [16] L. Tedeschini-Lalli, and J. A. Yorke, *Commun. Math. Phys* **106**, 635 (1986).
- [17] U. Feudel, and C. Grebogi, *Chaos* **7**, 597 (1997); *ibid*, *Phys. Rev. Lett.* **91**, 134102 (2003).
- [18] C. Grebogi, H. E. Nusse, E. Ott, and J. A. Yorke, *in Lectures Notes in Mathematics* **1342**, 220 Ed by J. C. Alexander, Springer-Verlag, New York, 1988. See also references therein.
- [19] C. Grebogi, S. W. McDonald, E. Ott, and J. A. Yorke, *Phys. Lett* **99A**, 415 (1983).
- [20] The numerical simulations for $\varepsilon \leq 10^{-13}$ were carried out with high precision by using the MPFR C library for arbitrary precision [21], which seemed to be the best choice for trigonometric functions. However, the computational cost is relatively high in comparison to standard C precision. For the exponent uncertainty, we have iterated a sufficient number of initial conditions, in order to reach 400 uncertain points. Using standard precision, we have fixed this limit up to 10000.
- [21] L. Fousse, G. Hanrot, V. Lefèvre, P. Pélissier, and P. Zimmermann, MPFR: A multiple-precision binary floating-point library with correct rounding. *ACM Trans. Math. Softw.* **33**, 13 (2007).
- [22] Effective fractal dimension has been defined in a similar way for Hamiltonian system [7].
- [23] D. Ruelle, *Comm. in Mathematical Physics* **82**, 137 (1981).
- [24] In fact this definition is general for a C^r -diffeomorphism $f : M \rightarrow M$, where M is some smooth manifold.
- [25] H. E. Nusse, and J. A. Yorke. *Ergod. Th. & Dynam. Sys.*, 17:463, 1997; H. E. Nusse, and J. A. Yorke. *Physica D*, 90: 242, 1996; H. E. Nusse, and J. A. Yorke. *Phys. Rev. Lett.*, 84: 627, 2000;